

Microsupercapacitors Working at 250 °C

Viktoria Mishukova,^[a] Yingchun Su,^[a] Shiqian Chen,^[a] Nicolas Boulanger,^[b] Bo Xu,^[c] Hari Hara Sudhan Thangavelu,^[d] Jinhua Sun,^[d] Wei Xia,^[e] Alexandr Talyzin,^[b] and Jiantong Li^{*[a]}

The raised demand for portable electronics in high-temperature environments ($>150\text{ }^\circ\text{C}$) stimulates the search for solutions to release the temperature constraints of power supply. All-solid-state microsupercapacitors (MSCs) are envisioned as promising on-chip power supply components, but at present, nearly none of them can work at temperature over 200 °C, mainly restricted by the electrolytes which possess either low thermal stability or incompatible fabrication process with on-chip integration. In

this work, we have developed a novel process to fabricate highly thermally stable ionic liquid/ceramic composite electrolytes for on-chip integrated MSCs. Remarkably, the electrolytes enable MSCs with graphene-based electrodes to operate at temperatures as high as 250 °C with a high areal capacitance ($\sim 72\text{ mF cm}^{-2}$ at 5 mVs^{-1}) and good cycling stability (70% capacitance retention after 1000 cycles at 1.4 mA cm^{-2}).

Introduction

Due to their high power density and long cycle life, supercapacitors are envisioned as promising energy storage devices in various next-generation electronic products such as portable^[1] and wearable^[2] electronics, electric vehicles,^[3,4] sensors,^[5,6] and space devices.^[7,8] In particular, with the continuous miniaturization of electronics, planar on-chip microsupercapacitors (MSCs) have increasingly attracted more and more interest. The present MSCs are generally designed to operate in ambient environments lacking a significant thermal budget.

However, many emerging applications, such as aerospace, automotive, and oil drilling, require electronic and power modules to withstand temperatures $>150\text{ }^\circ\text{C}$.^[9] For example, on-wheel or on-engine sensors in automotive electronics must operate in a range of 150–250 °C.^[10] Unfortunately, so far none of the MSCs can work at temperature higher than 200 °C.^[11]

Supercapacitors are mainly composed of two sets of electrodes (anode and cathode), current collectors, electrolyte, and mesoporous separator. To operate in a high-temperature environment, all these components, along with the entire device structure, must possess sufficient thermal stability to maintain their electrochemical performance. Among them, the electrolyte has become the limiting factor for high-temperature operation.^[12] Conventionally, liquid electrolytes are desired due to their fast ion transport and good wetting properties.^[13] However, the commonly used organic solvents such as acetonitrile, propylene carbonate, ethylene carbonate, and diethyl carbonate can ignite at high temperature and pose a potential fire hazard. Aqueous liquid electrolytes can tolerate only temperatures around 100 °C. For example, supercapacitors using “water-in-salt” electrolytes can only operate at temperatures up to 120 °C.^[14] Alternatively, solid-state electrolytes (SSEs) are a good option for mechanically robust, and thermally and chemically stable devices. Many efforts were made to develop a variety of SSEs, including polymer, ceramic, and ceramic-polymer SSEs.^[11] Typically, polymer SSEs are composed of a polymer matrix embedded with acid, alkaline or salt solute.^[15] Their thermal stability is primarily determined by the chosen polymer and has been reported to withstand temperatures up to 150 °C.^[16] Ceramic electrolytes have excellent thermal and mechanical properties and have enabled devices to operate at temperature over 300 °C.^[17–20] However, their electrochemical performance is significantly degraded by the low ionic conductivity and the increased interfacial resistance with the electrodes, resulting in low specific capacitance^[20] and/or limited rate capability.^[19] Another drawback is their brittleness and poor processability, which considerably slows down

- [a] V. Mishukova, Dr. Y. Su, S. Chen, Prof. J. Li
KTH Royal Institute of Technology
School of Electrical Engineering and Computer Science
Electrum 229, 164 40 Kista (Sweden)
E-mail: jiantong@kth.se
- [b] Dr. N. Boulanger, Prof. A. Talyzin
Department of Physics
Umeå University
901 87 Umeå (Sweden)
- [c] Prof. B. Xu
MIIT Key Laboratory of Advanced Display Materials and Devices
Institute of Optoelectronics & Nanomaterials
School of Materials Science and Engineering
Nanjing University of Science and Technology
210 094 Nanjing (China)
- [d] H. H. S. Thangavelu, Prof. J. Sun
Department of Industrial and Materials Science
Chalmers University of Technology
412 58 Gothenburg (Sweden)
- [e] Prof. W. Xia
Applied Materials Science
Department of Materials Science and Engineering
Uppsala University
751 21 Uppsala (Sweden)

 © 2023 The Authors. *Batteries & Supercaps* published by Wiley-VCH GmbH. This is an open access article under the terms of the Creative Commons Attribution Non-Commercial NoDerivs License, which permits use and distribution in any medium, provided the original work is properly cited, the use is non-commercial and no modifications or adaptations are made.

the implementation of such electrolytes for on-chip integration. In contrast, with the addition of polymer to the system, the resultant ceramic-polymer electrolyte can overcome these shortcomings, but then again at the expense of thermal stability.^[12] On the other hand, room temperature ionic liquids (RTILs) have received increasing interest in the fields of high-temperature supercapacitors due to their high thermal stability (up to around 300–400 °C), low toxicity and large electrochemical potential window.^[17] After integrating with a solid matrix, such as ceramic nanoparticles, polymer and clay,^[16,21,22] RTILs form solid-state ionogels that exhibit much higher ionic conductivity than pure ceramic electrolytes. As a result, ionogels have enabled supercapacitors to operate at up to 200 °C with large specific capacitance (> 100 F g⁻¹)^[21] and high rate capability (> 100 mV s⁻¹).^[16,22]

Compared with the sandwiched device structure in conventional supercapacitors, the planar structure in MSCs is meritorious for high-temperature operation because it does not need any membrane separators. However, the extra challenge for fabricating high-temperature MSCs primarily arises from the incompatibility of most present high-temperature electrolyte fabrication with on-chip integration. For example, the fabrication of ceramic electrolytes requires high-temperature (> 600 °C) processing,^[19] while many on-chip electronic devices can only sustain temperature up to 400 °C.^[23] Moreover, their need for high-pressure pressing could also be problematic for many electronic chips. Meanwhile, the “structural stability” of the entire electrolyte under high temperature could also influence the operating temperature limit of the MSCs. For example, all

the individual materials in ionogels (such as RTILs, ceramic nanoparticles, and clays) possess high thermal stability over 300 °C, whereas so far the highest operating temperature for ionogel-based supercapacitors is merely 200 °C.^[11] When it comes to MSCs, to our best knowledge, the reported highest operating temperature is no more than 150 °C.^[16] A possible reason could be the deformation of the electrolyte (and/or electrode) structures under the harsh operating environment, even though the corresponding electrolyte/electrode materials likely remain intact.

In this work, we have demonstrated a facile two-step assembly method to fabricate highly thermally stable ionic liquid/ceramic composite electrolytes that is compatible with on-chip integratable MSCs. In our process, slurry of calcium sulfate hemihydrate ($\text{CaSO}_4 \cdot \frac{1}{2}\text{H}_2\text{O}$), known as plaster of Paris,^[24] is first deposited onto graphene-based interdigitated planar electrodes and thermally treated to porous ceramic (CaSO_4) matrix, followed by the injection of RTIL into the ceramic matrix to form the final quasi-solid-state electrolytes (Figure 1). The method effectively avoids high-temperature or high-pressure processes, and the unfavorable interaction between the ceramic precursors and the ionic liquids, but synergistically combines the beneficial properties of liquid electrolytes (high ionic conductivity) and solid electrolytes (easy integration) to enable the fabrication of high-performance MSCs of areal capacitance over 72 mF cm⁻² (at scan rate of 5 mV s⁻¹) at a record operating temperature of 250 °C.

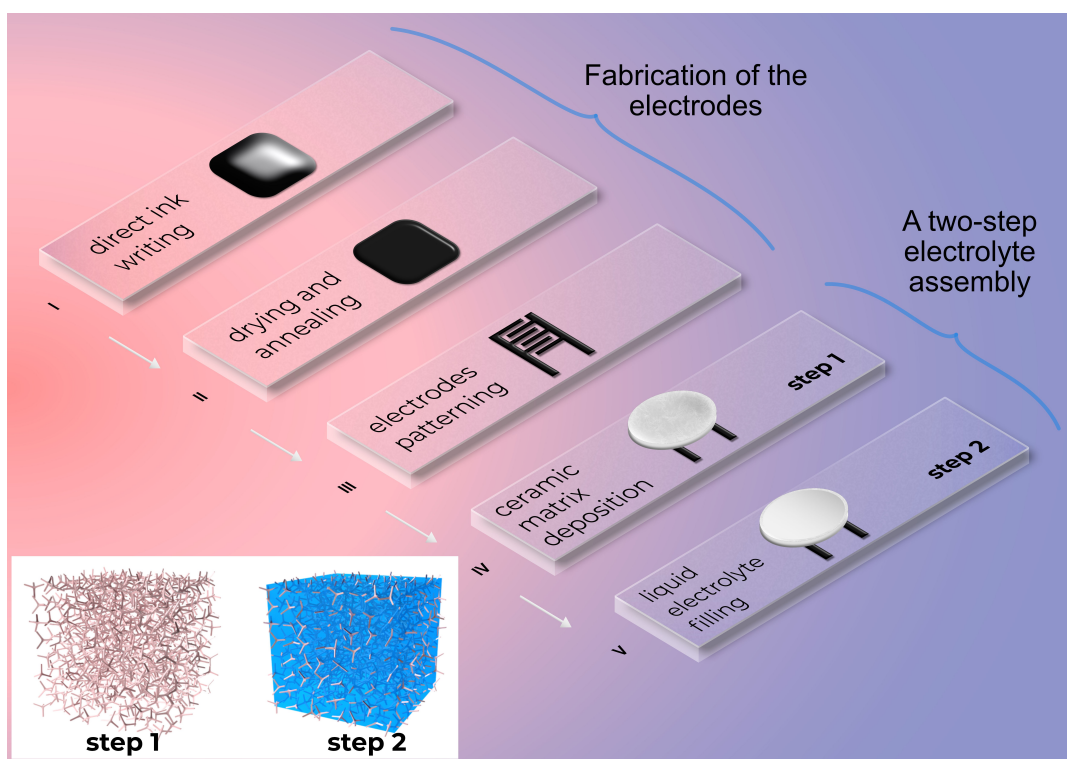


Figure 1. Schematic of the fabrication process flow of our high-temperature MSCs, (inset) Illustration of our two-step electrolyte assembly process model: a porous ceramic matrix is first fabricated in Step 1, followed by the injection of liquid electrolyte in Step 2.

Results and Discussion

In conventional fabrication of on-chip MSCs, solid-state electrolytes are formulated by first dissolving a matrix material (polymer, ceramic nanoparticles, etc.) in a liquid solvent with further addition of electrolyte solutes. The resulting electrolyte precursors are then applied, typically through drop casting or printing,^[25,26] to the MSC electrodes in “one step”, followed by drying into the solid-state (or gel-like) electrolyte. However, such one-step fabrication typically requires that both the electrolyte solutes and the matrix materials simultaneously disperse well in a common liquid. This greatly restricts the choice of compatible matrix materials and electrolyte solutes to develop advanced electrolytes of improved performance or extra functionality. In contrast, our electrolyte preparation relies on a two-step process (Figure 1). First, the precursor of the ceramic matrix, calcium sulfate hemihydrate in powder form (Figure 2d, e), is hydrated and transformed into a crystalline material with rod-like micro-crystals, which interlock between each other and generate a rigid and porous ceramic matrix with high structural stability (Figure 2f, g). After drying, a liquid electrolyte is injected into the porous ceramic matrix, where it stays confined without the need for encapsulation (Figure 2h). It is worth noting that benefiting from its high structural stability, the ceramic matrix does not undergo any structural

deformation during and after the filling of RTIL. This is the striking distinction between our electrolytes and ionogels. In this work, 1-butyl-3-methylimidazolium tetrafluoroborate (BMIM-BF₄) was chosen as the liquid electrolyte thanks to its excellent ionic conductivity, non-volatility and non-toxicity, high thermal stability up to 300–400 °C (according to thermogravimetric analysis in Ref. [27]), and high flash point of 288 °C. The stable ceramic matrix-confined liquid electrolytes constitute the quasi “solid-state” electrolytes to ensure the high performance of our activated graphene-based MSCs at high temperature. As shown in Figure 1, our high-temperature MSCs can then be fabricated in a facile process. First, conductive graphene inks are printed on glass substrates through direct ink writing, dried, annealed, and patterned into interdigitated structure through laser scribing. Then, the quasi-solid-state electrolytes are applied to the electrodes through the two-step assembly process. Throughout the MSC fabrication, neither high-temperature (>400 °C) nor high-pressing processes are needed.

To further underline the thermal stability of our MSCs and, specifically, the novel electrolyte, we performed the wide-angle X-ray scattering (WAXS) analysis of the porous ceramic matrix with and without the addition of ionic liquid electrolyte at different temperatures (Figure 3). The analysis has revealed several characteristic peaks. According to them, the overall

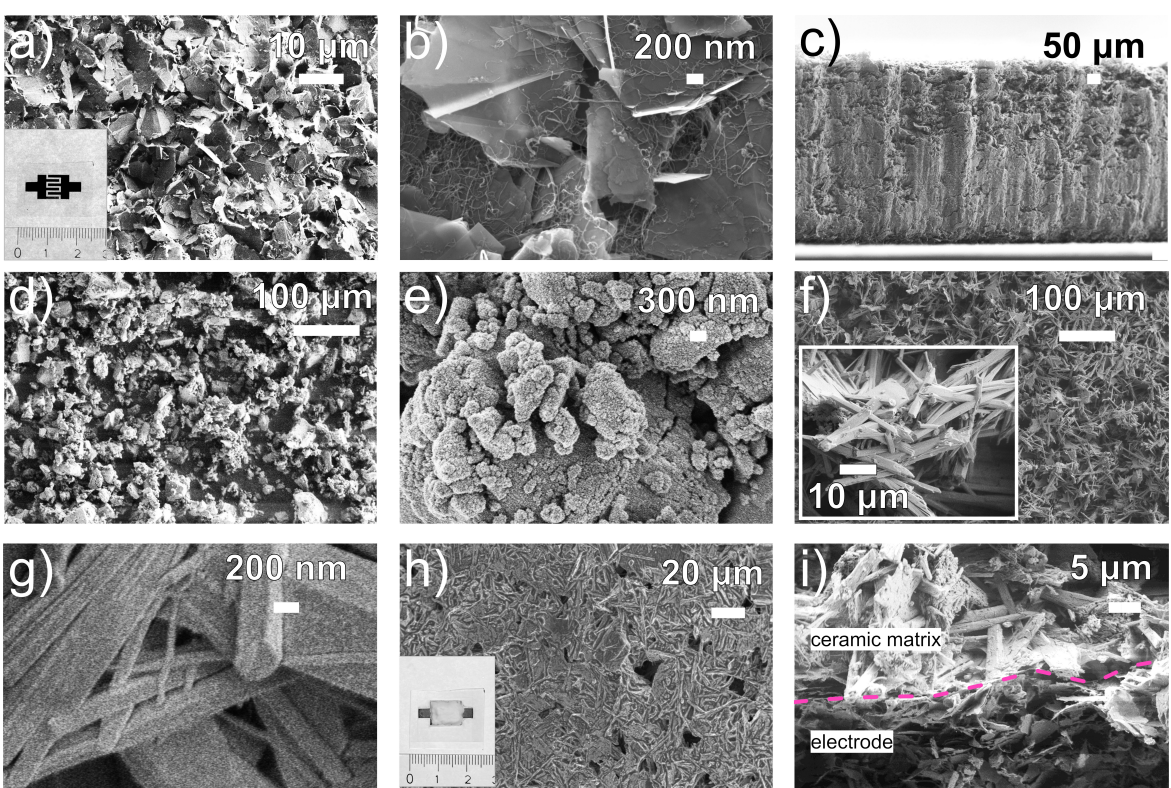


Figure 2. Morphology characterization (SEM images) of the components of the MSCs. a) Top surface of the graphene electrode, (inset) photograph of interdigitated graphene electrodes. b) High-resolution of the top surface of the graphene electrode demonstrating the presence of carbon nanotubes and large graphene flakes. c) Cross-section of the graphene electrode revealing its thickness of ~260 μm. d) Top view of the calcium sulfate hemihydrate powder. e) A close-up top view of grains of calcium hemihydrate powder. f) Top view of the hydrated calcium sulfate hemihydrate after drop casting onto graphene electrodes, (inset) Close-up view of the microstructure of ceramic matrix. g) High-resolution view of the morphology of drop cast ceramic matrix. h) Top view of the final quasi-solid-state electrolyte (ceramic matrix injected with liquid electrolyte), (inset) photograph of the final MSC. i) Cross-section of the ceramic matrix atop graphene electrodes.

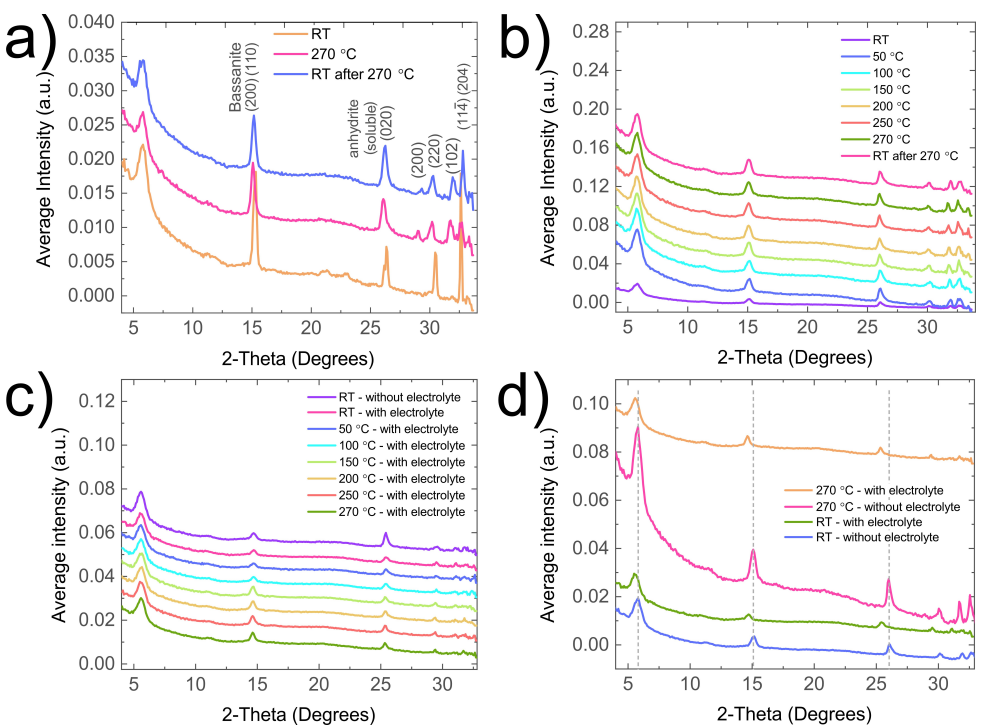


Figure 3. WAXS patterns of the ceramic matrix for the quasi-solid-state electrolyte. a) The hydrated calcium sulfate hemihydrate powder before and after heat treatment. b) The solid-state ceramic matrix (without electrolyte) at temperatures increasing from room temperature up to 270 °C. c) The solid-state ceramic matrix with injected ionic liquid electrolyte at temperatures up to 270 °C. d) The ceramic matrix with and without the ionic liquid electrolyte at room temperature and 270 °C.

ceramic matrix, after heating, could be a mixture of hydrous and anhydrite forms of calcium sulfate. Anyway, after the exposure to temperatures up to 270 °C (Figure 3b), there is no change in the crystalline structure. Even with the addition of the ionic liquid electrolyte, the WAXS peaks still remain unchanged (Figure 3c), which displays excellent temperature stability of our electrolyte. The observed shift in the WAXS peaks after the addition of the ionic liquid (Figure 3d) is likely caused by penetration of the electrolyte into the crystal lattice of the porous matrix that increases the crystal plane distance, while the overall crystal structure remains intact.

The electrochemical performance of the MSCs was characterized at high temperature to further evaluate their thermal stability. Cyclic voltammetry (CV), electrochemical impedance spectroscopy (EIS) and galvanostatic charge/discharge (GCD) of the MSCs were studied at temperatures ranging from 25 to 250 °C. Figure 4(a-c) shows the CV curves for the MSCs at various scan rates. The presence of a rectangular shape of the CV curves at low scan rates (Figure 4c) points to the electrical-double layer capacitive behavior of the MSCs.^[29] At high scan rates up to 250 mV s⁻¹, the CV profiles become lens-like at 25 °C (Figure 4a), whereas they retain good rectangularity at 250 °C (Figure 4b), indicating the effective operation and high rate capability of the MSCs at the record temperature of 250 °C. Noticeably, as shown in Figure 4(d), at 250 °C, a high areal capacitance is attained of 72 mF cm⁻² at 5 mV s⁻¹ (equivalent to a volumetric capacitance of 2.8 F cm⁻³), corresponding to an areal energy density of 10 µWh cm⁻² and an areal power density

of 0.5 mW cm⁻² (equivalent to volumetric energy density 0.4 mWh cm⁻³ and power density of 19 mW cm⁻³). The areal capacitance can still be retained at ~10 mF cm⁻² even when the scan rate increases to 250 mV s⁻¹. The values are much higher than other stacked (non-planar) supercapacitors in the literature^[20,30] operated at temperature about 200–220 °C. The high areal capacitance of our MSCs should originate from the improved interfacial compatibility of the novel electrolyte, as well as the 3D printed thick (>200 µm, Figure 2c) activated graphene electrodes that possess very large surface area (~2700 m² g⁻¹).^[16] One should note that the electrochemical performance strongly depends on the operating temperature, as shown in Figure 4(d, e). With the temperature increasing from 25 °C to 250 °C, the areal capacitance increases from 15 to 72 mF cm⁻² (Figure 4d) and, meanwhile, the equivalent series resistance decreases from 735 Ohm cm² to 27 Ohm cm² (Figure 4e). The reason for the improved electrochemical performance at high temperatures is well known and could be ascribed to the decreased viscosity of the ionic liquid, which improves wetting of the electrode,^[28] increases the ionic mobility and hence the ionic conductivity.^[27] Therefore, it can be inferred that the ionic conductivity of our quasi-solid-state electrolytes is dominated by the viscosity of the ionic liquid, not limited by the ceramic matrix itself. This implies the effectiveness of our two-step assembly process for the fabrication of high-temperature electrolytes. More importantly, the MSCs exhibited good stability under the temperature cycling test (Figure 4f). In each cycle, the MSCs at 250 °C were cooled down to room temper-

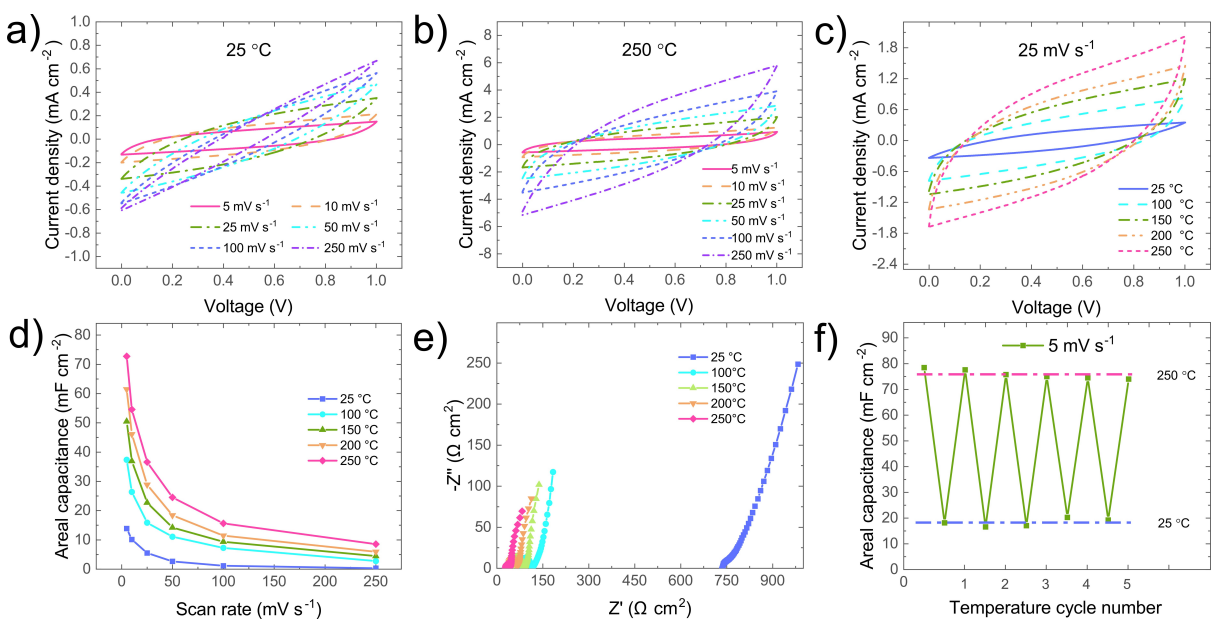


Figure 4. Electrochemical performance of the high-temperature MSCs. a, b) CV curves at different scan rates at a) 25 °C and b) 250 °C. c) CV curves at a scan rate of 25 mV s⁻¹ at various temperature. d) Areal capacitance calculated from the CV curves at different temperature and scan rate. e) Nyquist plot of the MSCs at different temperature. f) Areal capacitance of the MSCs measured at temperature varying between 250 and 25 °C for 5 cycles.

ature and then heated up again to 250 °C. After multiple cycles, their capacitance could still keep at the constant values with very little variation at both temperatures (10% at 25 °C and 6% at 250 °C), suggesting the excellent thermal stability and recoverability of the quasi-solid-state electrolytes.

As shown in Figure 5, under the optimized test conditions, the GCD curves are nearly symmetrical and triangular (Figure 5a, b), further confirming the good capacitive behavior of our high-temperature MSCs. Certainly, at a low temperature of 25 °C, the MSCs exhibit a high IR drop of about 0.3 V even at a low current density of 50 $\mu\text{A cm}^{-2}$, resulting from the large resistance (Figure 4e), which is likely caused by high viscosity of the RTIL. Nevertheless, with increasing temperatures, the IR drop decreases significantly (Figure 5c). At 250 °C, the IR drop is only around 0.1 V even at a current density as high as 1400 $\mu\text{A cm}^{-2}$ (Figure 5b). When the temperature increases from 100 °C to 250 °C (Figure 5e), the areal capacitance increases from $\sim 10 \text{ mF cm}^{-2}$ to $\sim 40 \text{ mF cm}^{-2}$. Compared to the CV tests, the MSCs attained the highest areal capacitance of 44.6 mF cm^{-2} at 250 °C and 800 $\mu\text{A cm}^{-2}$. At each temperature (Figure 5e), the areal capacitance degrades very slowly with the increasing current density (even up to 1400 $\mu\text{A cm}^{-2}$), implying the high rate capability of our MSCs. The cycling behavior of the MSCs (Figure 5f) indicates a capacitance retention of 68.5% at 250 °C after 1000 cycles at 1400 $\mu\text{A cm}^{-2}$. To the best of our knowledge, this should be the first demonstration of the cycling performance of MSCs at a high temperature of 250 °C. The relatively low capacitance retention is likely caused by the long test time (about 12 hours), rather than the intrinsic degradation of the thermal stability of the MSCs. Due to the lack of encapsulation, the long-time exposure of the MSCs at 250 °C could induce significant evaporation (as shown in Figure 5h, i)

of the ionic liquid BMIM-BF₄ (whose boiling point is about 280 °C, close to the operating temperature), and hence lower the areal capacitance. It is expected that proper encapsulation could prevent the ionic liquid evaporation and greatly increase the cycling performance.

Typically, the voltage supplied by a single MSC is inadequate to operate practical electronic circuits. To achieve a desired voltage, connecting several MSCs in series is often required.^[31] Benefiting from the scalability of our fabrication process (Figure 1), it is straightforward to fabricate MSC arrays with both electrodes and interconnect made of graphene (Figure 6a). Figure 6(b) shows the CV and GCD curves of three MSCs connected in series at 250 °C with a voltage window of 3 V. As compared with the single MSC (Figure 6b, c), the MSC array exhibits approximately scalable capacitive behavior. To the best of our knowledge, this is the first demonstration of a series connection of multiple MSCs operating at 250 °C.

Finally, Figure 7 compares the temperature-dependent areal capacitance of our MSCs with that of the high-temperature stacked supercapacitors and MSCs published in the literature.^[16,30,33–40] It is clear that our MSCs have attained a record operating temperature of 250 °C for MSCs and meanwhile exhibit areal capacitance ($> 70 \text{ mF cm}^{-2}$) much higher than that of most other supercapacitors (including both stacked supercapacitors and planar MSCs). In addition to the improved performance, the simplicity and scalability of our two-step assembly process make it a generic and promising strategy to fabricate quasi-solid-state electrolytes for high-temperature on-chip MSCs.

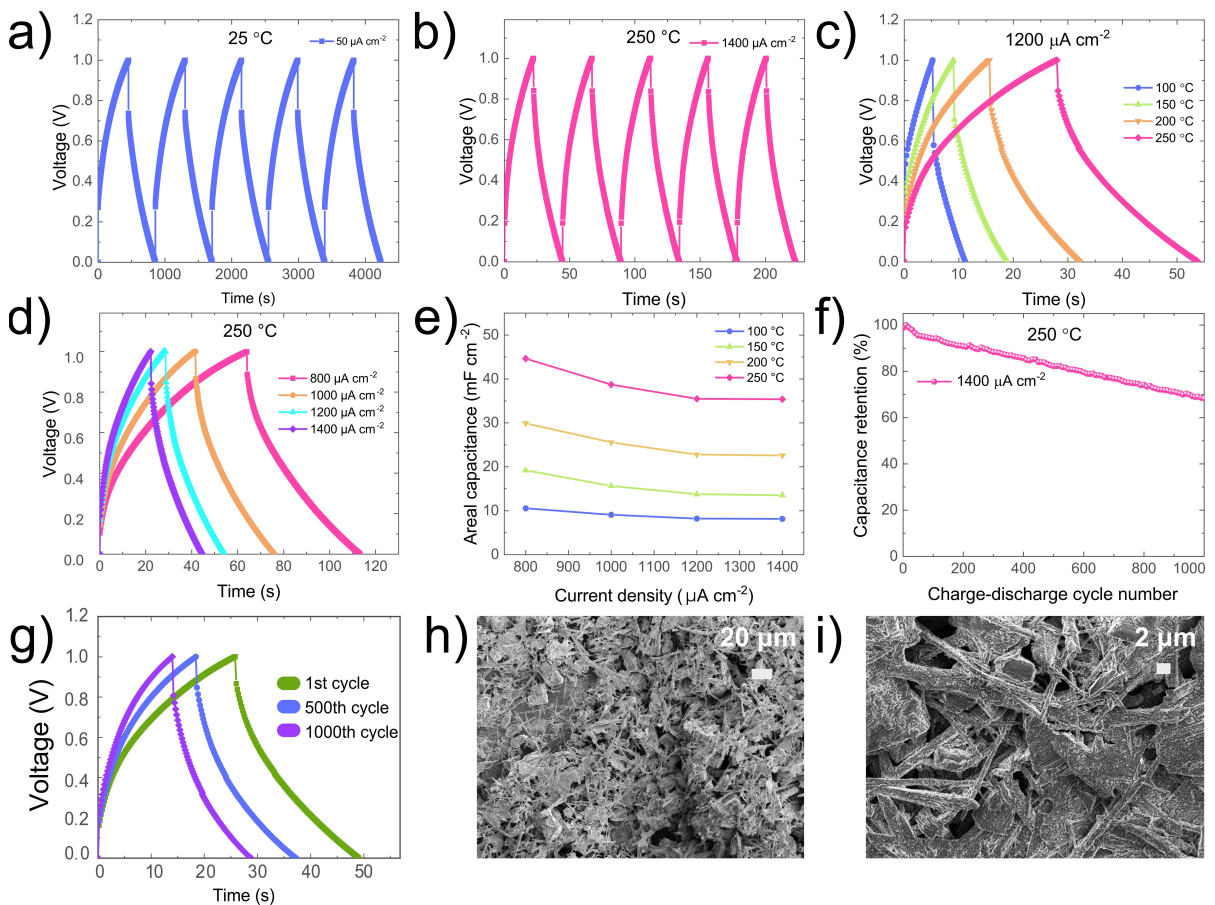


Figure 5. GCD characterization of the high-temperature MSCs. a, b) GCD curves at different current densities at a) 25 °C and b) 250 °C. c) GCD curves at different temperatures at the current density of 1200 $\mu\text{A cm}^{-2}$. d) GCD cycles at 250 °C at different current density. e) Current density-dependent areal capacitance at various temperature. f) Capacitance retention of the MSCs during the GCD tests at 1400 $\mu\text{A cm}^{-2}$ at 250 °C. g) GCD curves after different cycle numbers. h, i) SEM images of the top view of the quasi-solid-state electrolytes after 1000 GCD cycles at 250 °C.

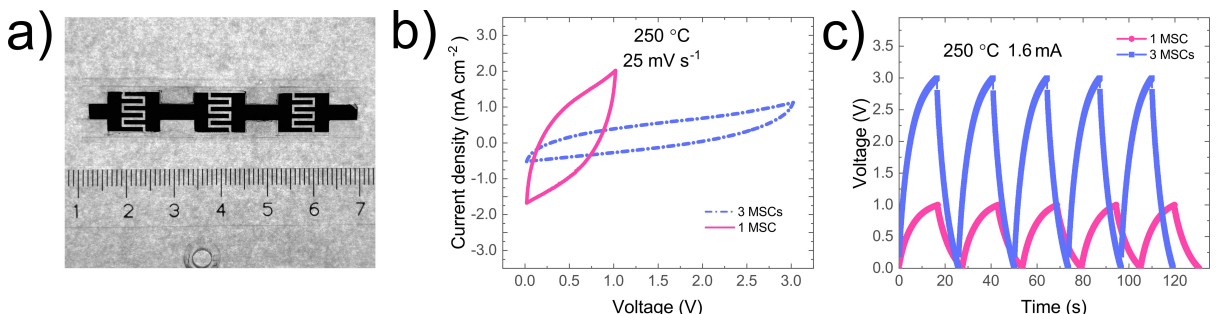


Figure 6. Electrochemical performance of the high-temperature MSC arrays. a) Photograph of an MSC array consisting of 3 MSCs connected in series. b) CV curves at 25 mV s^{-1} and c) GCD curves at 1.6 mA of the MSC array in (a) operating at 250 °C, in comparison with the one single MSC (a charging current of 1.6 mA corresponds to a current density of 2 mA cm^{-2} for a single device).

Conclusions

In conclusion, our novel two-step assembly of the quasi-solid-state electrolyte has enabled the fabrication of planar MSCs of temperature tolerance up to 250 °C. The hydration of calcium sulfate hemihydrate and subsequent thermal treatment result in the robust porous ceramic matrix which can confine ionic liquid to form thermal-stable quasi-solid-state electrolytes. The elec-

trolytes enable facile and scalable fabrication of on-chip MSCs with graphene electrodes to operate at a record high temperature of 250 °C with high areal capacitance $> 70 \text{ mF cm}^{-2}$. The performance is evidently higher than that of almost all other MSCs in the literature, in terms of both areal capacitance and operating temperature. Likely for the first time, we have demonstrated that the MSCs can retain 68.5% of its capacitance after 1000 cycles of charge and discharge at 250 °C. Also, for the

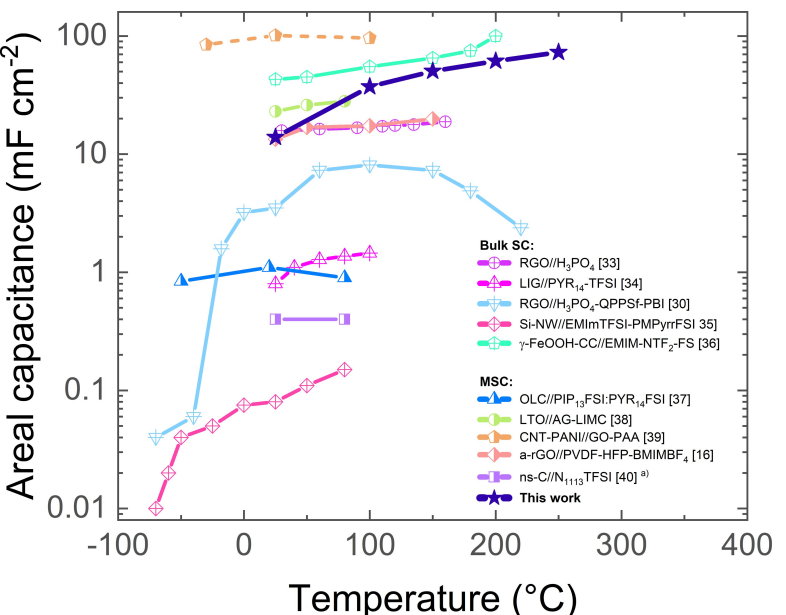


Figure 7. The areal capacitance of the high-temperature MSCs compared with other reported supercapacitors^[16,30,33–40] operating in a wide temperature window, including stacked supercapacitors and planar MSCs. ^{a)} The reference provides volumetric capacitance, which is converted to areal capacitance, based on the electrode thickness provided therein.

first time, multiple MSCs have been connected in series to operate at a high voltage window of 3 V at 250°C. The demonstrated two-step assembly process of electrolytes is promising for on-chip integration of MSCs for high-temperature electronics.

Experimental Section

Graphene ink formulation. The graphene ink was formulated by using the combination of 300 mg carbon black (dispersed in water, solid amount 5%, Jiangsu XFNANO Materials Tech Co., China) and 150 mg of our previously reported activated graphene.^[31] First, the carbon black dispersion was washed with acetone via centrifugation twice to remove the solvent (water) and binders, and then the collected carbon black sediment was mixed with our activated graphene inks. The mixture was centrifuged at 10 000 rpm for 20 minutes to remove the solvent (water). Finally, 7.5 mL of 80 mg mL⁻¹ ethyl cellulose in terpineol was added and stirred at 200 rpm for 1 hour at 90°C, followed by stirring at 1000 rpm overnight to form uniform viscous graphene inks that suit well for direct ink writing.

MSC electrode fabrication. The fabrication of the MSC electrodes starts with 3D printing (direct ink writing) of thick graphene films (200–300 µm) in rectangular shapes with a total area of 1.2 cm² for individual MSCs (the MSC arrays need up-scaled electrode area, including the interconnects) through Felix 3D bioprinter (FELIX-printers, Netherlands). The glass slide substrate was pre-cleaned in acetone, followed by isopropanol under sonication in an ultrasonic bath for 10 minutes. After printing, the ink was dried for 6 hours at room temperature inside a fume hood, followed by 1 hour drying at 65°C, and a two-step annealing at 200°C for 30 minutes and at 350°C for 1 hour. The resulting graphene films were patterned by pulsed fiber laser (120–150 ns at 30 kHz, pulsed repetition rate 30–60 kHz, λ = 1064 nm) with a beam power of 6 W to shape two interdigitated electrodes designed with six 1-mm-wide fingers, an

inter-finger gap of 500 µm and a total footprint area of 0.88 cm². After patterning, the structures were lightly blown with a stream of nitrogen gas to remove all the residual vaporized particles and the surrounding area was wiped with ethanol. Finally, the electrical resistance between the two electrodes was measured to ensure open circuits.

Electrolyte fabrication. Calcium sulfate hemihydrate (VWR, Sweden) was mixed with deionized water (weight ratio 1:1) in a 30 mL glass vial and stirred for 1 minute, followed by setting still for 11 minutes. Then for each individual MSC, 200 µL of the hydrated mixture was drop cast onto the interdigitated electrodes and dried at room temperature for 6 hours, followed by annealing at 270°C for 15 minutes. Finally, 60 µL of ionic liquid BMIM-BF₄ (≥ 97.0% (HPLC), Merck) was drop cast onto the ceramic matrix, followed by heating up the device at 250°C for 10 minutes to ensure sufficient penetration of the electrolyte into the ceramic matrix.

Characterization. High-temperature electrochemical analyses (CV, EIS, and GCD) were performed using Gamry Interface 1010E potentiostat (Gamry Instruments Inc., Warminster PA, USA) in combination with Signatone S-1060R 4" Hot Chuck probe station. Scanning electron microscopy (SEM, Zeiss Gemini Ultra 55) was used for morphology characterization of the materials and devices. The WAXS patterns of the ceramic matrix materials at elevated temperature were obtained using the Mat:Nordic instrument from SAXSLAB with the X-ray wavelength of 1.54056 Å.

The areal capacitance was extracted from cyclic voltammetry curves as in $C_{A,CV} = \frac{\int_{A_0}^{\Delta V} (I_C - I_D)dV}{2A_0\Delta V}$, where ΔV is the voltage window, I_C is the charging current, I_D is the discharging current, A is the device area including inter-finger space, and v is the scan rate. The areal capacitance was extracted from GCD characteristics using $C_{A,GCD} = \frac{|I_D|\Delta t}{A\Delta V}$ where Δt is the discharging time. The corresponding areal energy density E_D and areal power density P_D were calculated using $E_D = \frac{C_{A,CV}\Delta V^2}{2}$, $P_D = \frac{E_D}{\Delta V/v}$ respectively.

Acknowledgements

We acknowledge the financial support of the Swedish Research Council (Grant No. 2019-04731 and 2020-04341), the Swedish Foundation for International Cooperation in Research and Higher Education (STINT, CH2017-7284), and the Swedish Agency for Innovation Systems (Vinnova, 2021-04030). A.T. acknowledges funding from the European Union's Horizon 2020 Research and Innovation Program (Grant No. 881603) and Energimyndigheten (Grant No. 50620-1).

Conflict of Interests

The authors declare no conflict of interest.

Data Availability Statement

The data that support the findings of this study are available from the corresponding author upon reasonable request.

Keywords: microsupercapacitors • high temperature electronics • solid electrolytes • ceramic matrix • ionic liquid

- [1] W. Si, C. Yan, Y. Chen, S. Oswald, L. Han, O. G. Schmidt, *Energy Environ. Sci.* **2013**, *6*, 3218.
- [2] K. Keum, J. W. Kim, S. Y. Hong, J. G. Son, S. S. Lee, J. S. Ha, *Adv. Mater.* **2020**, *32*, 2002180.
- [3] S. Hérou, J. J. Bailey, M. Kok, P. Schlee, R. Jervis, D. J. L. Brett, P. R. Shearing, M. Crespo Ribadeneyra, M. Titirici, S. Hérou, P. Schlee, M. C. Ribadeneyra, M. Titirici, J. J. Bailey, M. Kok, R. Jervis, D. J. L. Brett, R. Shearing, *Adv. Sci.* **2021**, *8*, 210016.
- [4] R. R. Salunkhe, Y. H. Lee, K. H. Chang, J. M. Li, P. Simon, J. Tang, N. L. Torad, C. C. Hu, Y. Yamauchi, *Chem. Eur. J.* **2014**, *20*, 13838.
- [5] Y. Lee, V. K. Bandari, Z. Li, M. Medina-Sánchez, M. F. Maitz, D. Karnaushenko, M. V. Tsurkan, D. D. Karnaushenko, O. G. Schmidt, *Nat. Commun.* **2021**, *12*, 4967.
- [6] L. Gao, Y. Wang, X. Hu, W. Zhou, K. Cao, Y. Wang, W. Wang, Y. Lu, *ACS Appl. Mater. Interfaces* **2019**, *11*, 26288.
- [7] J. Gonzalez-Llorente, A. A. Lidtke, K. Hatanaka, L. Limam, I. Fajardo, K. I. Okuyama, *Acta Astronaut.* **2020**, *174*, 294.
- [8] K. C. Chin, N. W. Green, E. J. Brandon, *J. Power Sources* **2018**, *379*, 155.
- [9] J. Watson, G. Castro, *J. Mater. Sci. Mater. Electron.* **2015**, *26*, 9226.
- [10] X. Lin, M. Salari, L. M. R. Arava, P. M. Ajayan, M. W. Grinstaff, *Chem. Soc. Rev.* **2016**, *45*, 5848.
- [11] V. Kumaravel, J. Bartlett, S. C. Pillai, *Adv. Energy Mater.* **2021**, *11*, 2002869.
- [12] L. Fan, S. Wei, S. Li, Q. Li, Y. Lu, *Adv. Energy Mater.* **2018**, *8*, 1702657.
- [13] F. Béguin, E. Frackowiak, *Supercapacitors: Materials, Systems, and Applications*, Wiley, 2013.
- [14] L. W. Le Fevre, A. Ejigu, R. Todd, A. J. Forsyth, R. A. W. Dryfe, *Chem. Commun.* **2021**, *57*, 5294.
- [15] H. Dai, G. Zhang, D. Rawach, C. Fu, C. Wang, X. Liu, M. Dubois, C. Lai, S. Sun, *Energy Storage Mater.* **2021**, *34*, 320.
- [16] V. Mishukova, N. Boulanger, A. Iakunkov, S. Sollami Delektka, X. Zhuang, A. Talyzin, J. Li, *Nanoscale Adv.* **2021**, *3*, 4674.
- [17] R. S. Borges, A. L. M. Reddy, M.-T. F. Rodrigues, H. Gullapalli, K. Balakrishnan, G. G. Silva, P. M. Ajayan, *Sci. Rep.* **2013**, *3*, 2572.
- [18] N. Brambilla, F. Martini, *Trans.-Geotherm. Resour. Coun.* **2015**, *39*, 1065.
- [19] T. Hakari, S. Yoshimi, K. Nagao, A. Sakuda, M. Tatsumisago, A. Hayashi, *J. Power Sources* **2022**, *543*, 231821.
- [20] C. H. Chang, B. Hsia, J. P. Alper, S. Wang, L. E. Luna, C. Carraro, S. Y. Lu, R. Maboudian, *ACS Appl. Mater. Interfaces* **2015**, *7*, 26658.
- [21] X. Liu, O. O. Taiwo, C. Yin, M. Ouyang, R. Chowdhury, B. Wang, H. Wang, B. Wu, N. P. Brandon, Q. Wang, S. J. Cooper, *Adv. Sci.* **2019**, *6*, 1801337.
- [22] H. H. Rana, J. H. Park, E. Ducrot, H. Park, M. Kota, T. H. Han, J. Y. Lee, J. Kim, J. H. Kim, P. Howlett, M. Forsyth, D. MacFarlane, H. S. Park, *Energy Storage Mater.* **2019**, *19*, 197.
- [23] J. Jeong, D. M. Geum, S. H. Kim, *Electronics* **2022**, *11*, 3013.
- [24] S. Svorová Pawełkowicz, P. Svara, Z. Prošek, M. Keppert, E. Vejmelková, N. Murafa, T. Sawoszczuk, J. Sygula-Cholewińska, H. Bíbová, *Constr. Build. Mater.* **2022**, *346*, 128426.
- [25] X. Aeby, A. Poulin, G. Siqueira, M. K. Hausmann, G. Nyström, *Adv. Mater.* **2021**, *33*, 2101328.
- [26] S. Sollami Delektka, M. M. Laurila, M. Mäntysalo, J. Li, *Nano-Micro Lett.* **2020**, *12*, 40.
- [27] S. K. Shalu Chaurasia, R. K. Singh, S. Chandra, *J. Phys. Chem. B* **2013**, *117*, 897.
- [28] M. Brachet, D. Gaboriau, P. Gentile, S. Fantini, G. Bidan, S. Sadki, T. Brousse, J. Le Bideau, *J. Mater. Chem. A* **2016**, *4*, 11835.
- [29] Z. Li, V. Ruiz, V. Mishukova, Q. Wan, H. Liu, H. Xue, Y. Gao, G. Cao, Y. Li, X. Zhuang, J. Weissenrieder, S. Cheng, J. Li, *Adv. Funct. Mater.* **2022**, *32*, 2108773.
- [30] A. Chaichi, G. Venugopalan, R. Devireddy, C. Arges, M. R. Gartia, *ACS Appl. Energ. Mater.* **2020**, *3*, 5693.
- [31] J. Li, S. Sollami Delektka, P. Zhang, S. Yang, M. R. Lohe, X. Zhuang, X. Feng, M. Östling, *ACS Nano* **2017**, *11*, 8249.
- [32] V. Skrypnichuk, N. Boulanger, A. Nordenström, A. Talyzin, *J. Phys. Chem. Lett.* **2020**, *11*, 3032.
- [33] S. K. Kim, H. J. Kim, J. C. Lee, P. V. Braun, H. S. Park, *ACS Nano* **2015**, *9*, 8569.
- [34] P. Zaccagnini, D. di Giovanni, M. G. Gomez, S. Passerini, A. Varzi, A. Lamberti, *Electrochim. Acta* **2020**, *357*, 136838.
- [35] R. Newell, J. Faure-Vincent, B. Iliev, T. Schubert, D. Aradilla, *Electrochim. Acta* **2018**, *267*, 15.
- [36] B. Shen, R. Guo, J. Lang, L. Liu, L. Liu, X. Yan, *J. Mater. Chem. A* **2016**, *4*, 8316.
- [37] P. Huang, D. Pech, R. Lin, J. K. McDonough, M. Brunet, P.-L. Taberna, Y. Gogotsi, P. Simon, J. K. McDonough, *Electrochim. Commun.* **2013**, *36*, 53.
- [38] S. Zheng, J. Ma, Z. S. Wu, F. Zhou, Y. B. He, F. Kang, H. M. Cheng, X. Bao, *Energy Environ. Sci.* **2018**, *11*, 2001.
- [39] X. Jin, G. Zhang, G. Sun, H. Yang, Y. Xiao, J. Gao, Z. Zhang, L. Jiang, L. Qu, *Nano Energy* **2019**, *64*, 103938.
- [40] L. G. Bettini, P. Piseri, F. De Giorgio, C. Arbizzani, P. Milani, F. Soavi, *Electrochim. Acta* **2015**, *170*, 57.

Manuscript received: July 16, 2023

Accepted manuscript online: July 20, 2023

Version of record online: July 20, 2023